ANTIOXIDANTS & REDOX SIGNALING
Volume 17, Number 10, 2012

DOI: 10.1089/ars.2011.4334

ORIGINAL RESEARCH COMMUNICATION

Peroxiredoxin III and Sulfiredoxin Together Protect Mice from Pyrazole-Induced Oxidative Liver Injury

Soo Han Bae,[1] Su Haeng Sung,[1] Hye Eun Lee,[1] Ha Tan Kang,[1] Se Kyoung Lee,[1] Sue Young Oh,[1] Hyun Ae Woo,[2] In Sup Kil,[1] and Sue Goo Rhee[1]

Abstract

Aims: To define the mechanisms underlying pyrazole-induced oxidative stress and the protective role of peroxiredoxins (Prxs) and sulfiredoxin (Srx) against such stress. ***Results:*** Pyrazole increased Srx expression in the liver of mice in a nuclear factor erythroid 2–related factor 2 (Nrf2)-dependent manner and induced Srx translocation from the cytosol to the endoplasmic reticulum (ER) and mitochondria. Pyrazole also induced the expression of CYP2E1, a primary reactive oxygen species (ROS) source for ethanol-induced liver injury, in ER and mitochondria. However, increased CYP2E1 levels only partially accounted for the pyrazole-mediated induction of Srx, prompting the investigation of CYP2E1-independent ROS generation downstream of pyrazole. Indeed, pyrazole increased ER stress, which is known to elevate mitochondrial ROS. In addition, pyrazole up-regulated CYP2E1 to a greater extent in mitochondria than in ER. Accordingly, among Prxs I to IV, PrxIII, which is localized to mitochondria, was preferentially hyperoxidized in the liver of pyrazole-treated mice. Pyrazole-induced oxidative damage to the liver was greater in PrxIII$^{-/-}$ mice than in wild-type mice. Such damage was also increased in Srx$^{-/-}$ mice treated with pyrazole, underscoring the role of Srx as the guardian of PrxIII. ***Innovation:*** The roles of Prxs, Srx, and ER stress have not been previously studied in relation to pyrazole toxicity. ***Conclusion:*** The concerted action of PrxIII and Srx is important for protection against pyrazole-induced oxidative stress arising from the convergent induction of CYP2E1-derived and ER stress-derived ROS in mitochondria. *Antioxid. Redox Signal.* 17, 1351–1361.

Introduction

The hepatotoxin pyrazole is a substrate of cytochrome P450 2E1 (CYP2E1). Similar to many other substrates for CYP2E1, pyrazole increases the expression of this enzyme at the level of protein stabilization (32). Such up-regulation of CYP2E1 results in oxidative stress, because electron transfer from the donor system to CYP2E1 is not perfectly coupled and is, therefore, leaky (27, 30), and the leaked electrons react with O_2 to produce reactive oxygen species (ROS). CYP2E1 is a major ROS producer that plays a central role in the pathogenesis of alcoholic liver injury (17, 20). Pyrazole has been widely used as an inducer of CYP2E1 in studies of CYP2E1-dependent oxidative stress and liver injury (21, 38, 39). Although CYP2E1 is predominantly localized to the endoplasmic reticulum (ER) (19), it is also present in mitochondria of the liver (1, 4, 24, 29). Pyrazole increases the abundance of CYP2E1 in both the ER and mitochondria of the rat liver (4, 29, 35).

Peroxiredoxins (Prxs) catalyze the reduction of ROS, with a catalytic cysteine (Cys) residue serving as the site of oxidation

Innovation

Pyrazole has been widely used as an inducer of CYP2E1 in studies of CYP2E1-dependent oxidative stress and liver injury. 2-cysteine peroxiredoxins (Prxs) (PrxI to IV) inevitably undergo hyperoxidation during the elimination of reactive oxygen species (ROS). Taking advantage of the fact that Prx isoforms reside in different subcellular compartments, the extent of hyperoxidation of each Prx isoform was measured to define the localization of ROS production. Here, we found that PrxIII, which is specifically localized to mitochondria, was preferentially hyperoxidized in the liver in response to exposure to pyrazole. This is likely because pyrazole increases CYP2E1 abundance to a greater extent in mitochondria than in the endoplasmic reticulum (ER) and because it induces ER stress that results in increased Ca^{2+} and ROS levels in mitochondria. Using mice lacking either PrxIII or sulfiredoxin, the pivotal function of the two enzymes in mitigating hepatotoxicity in pyrazole-treated mice was demonstrated.

[1]Division of Life and Pharmaceutical Sciences, Ewha Womans University, Seoul, Korea.
[2]Department of Bioinspired Sciences, College of Pharmacy, Ewha Womans University, Seoul, Korea.

by peroxides (28). The six mammalian Prx isoforms (PrxI to VI) show distinct subcellular distributions (12, 18, 28, 34). PrxI is located in the cytosol, in the plasma membrane, and at the cytosolic side of the ER membrane; PrxII and PrxVI are predominantly localized in the cytosol; PrxIV is restricted to the ER lumen; PrxV is present in the cytosol, mitochondria, and peroxisomes; and PrxIII is synthesized with a mitochondrial targeting sequence and is exclusively localized in the mitochondria. PrxI to PrxIV, the four members of the 2-Cys Prx subgroup, exist as homodimers and possess two conserved Cys residues. In the catalytic cycle of 2-Cys Prxs, peroxides oxidize the sulfhydryl group of the NH_2-terminal conserved Cys (designated the peroxidatic Cys, or C_P–SH) to Cys sulfenic acid (Cys–SOH), which then reacts with the COOH-terminal conserved Cys–SH (the resolving Cys, C_R–SH) of the other subunit in the homodimer to form a disulfide. The resulting disulfide is subsequently reduced by thioredoxin to complete the catalytic cycle. As a result of the slow rate of its reaction with C_R–SH, C_P–SOH is occasionally further oxidized to Cys sulfinic acid (Cys–SO_2H) (26, 40). This hyperoxidation reaction, which results in the inactivation of peroxidase function, is reversed by the ATP-dependent enzyme sulfiredoxin (Srx) (6,36,37).

We previously showed that chronic ethanol consumption in mice results in the hyperoxidation of PrxI, but not that of the other 2-Cys Prxs, in the liver (2). This specific inactivation of PrxI was due to the colocalization of a large proportion of PrxI molecules with CYP2E1 at the cytosolic side of the ER membrane. We now show that pyrazole induces hyperoxidation of the mitochondrial enzyme PrxIII, but not that of PrxI, in mouse liver, suggesting that ROS are predominantly produced by mitochondria in the liver of pyrazole-injected mice. The pronounced oxidative damage induced by pyrazole in mice lacking either Srx or PrxIII indicated that the concerted action of these enzymes is important for protection against the pyrazole-induced oxidative stress.

Results

Pyrazole upregulates Srx protein and mRNA in mouse liver via *an Nrf2-dependent pathway*

An intraperitoneal injection of mice with pyrazole at doses of 75, 150, or 300 mg/kg resulted in a marked increase in the amount of Srx protein in the liver measured 18 h later by immunoblot analysis, with this effect being maximal at the dose of 150 mg/kg (Supplementary Fig. S1; Supplementary Data are available online at www.liebertonline.com/ars). The abundance of Srx protein in the liver was increased ~17-fold by an injection of pyrazole at 150 mg/kg (Fig. 1A, B). Reverse transcription (RT) and real-time polymerase chain reaction (PCR) analysis also showed that pyrazole induced an ~22-fold increase in the amount of Srx mRNA in the liver (Fig. 1C). An immunohistochemical analysis revealed that Srx was localized around the central vein of the liver in pyrazole-injected mice (Fig. 1D). Immunoreactivity was detected in the cytoplasm and the nucleus (Fig. 1D), and the presence of a small fraction of Srx in the nucleus was confirmed by immunoblot analysis after subcellular fractionation (Fig. 1E).

Transcription of the Srx gene is regulated through a cis-acting element antioxidant-responsive element (ARE) that is activated by the binding of nuclear factor erythroid 2–related factor 2 (Nrf2) or activator protein-1 (AP-1). We previously

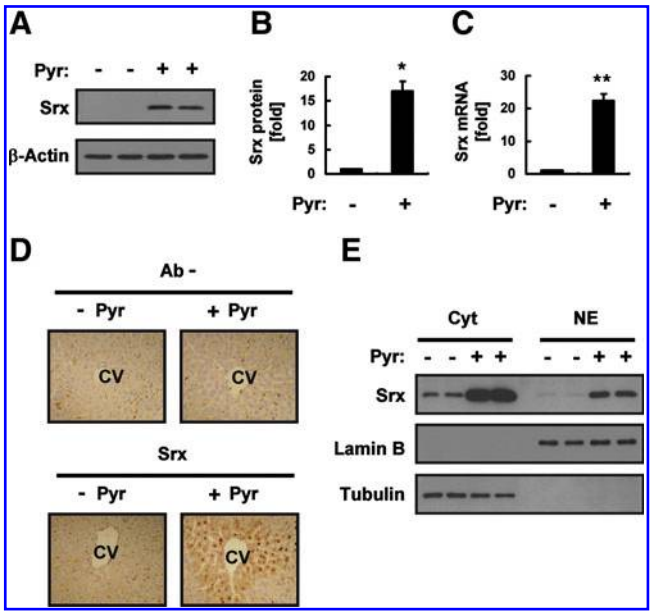

FIG. 1. Induction of sulfiredoxin (Srx) expression in the liver of mice treated with pyrazole (Pyr). (A) The liver of mice intraperitoneally injected with saline (−) or Pyr (150 mg/kg) was isolated 18 h after the injection, and liver homogenates (20 μg of protein) were subjected to an immunoblot analysis with antibodies to Srx or to β-actin (loading control). Data are representative of three independent experiments. **(B)** Densitometric analysis of Srx protein expression for the immunoblots similar to those in **(A)**. Data were normalized by the amount of β-actin and then expressed relative to the corresponding mean value for saline-injected mice. Data are mean ± standard deviation (SD). *$p < 0.01$ versus the saline group. **(C)** Total RNA prepared from the liver tissue of mice treated as in **(A)** was subjected to reverse transcription (RT) and real-time polymerase chain reaction (PCR) analysis for determination of the amounts of Srx mRNA. Data were normalized by the amount of 18S rRNA and then expressed relative to the corresponding value for saline-injected mice. Data are mean ± SD. **$p < 0.02$ versus the saline group. **(D)** Liver sections from mice treated as in **(A)** were subjected to an immunohistochemical analysis with or without antibodies (Ab−) to Srx with the use of an ABC staining kit (Vector Laboratories, Mississauga, Ontario, Canada). CV, central vein. Original magnification, 100×. **(E)** The cytosolic and nuclear fractions (20 μg of protein) prepared from the liver tissue of mice treated as in **(A)** were subjected to an immunoblot analysis with antibodies to Srx, to lamin B, or to tubulin. Data are representative of three independent experiments. (To see this illustration in color the reader is referred to the web version of this article at www.liebertpub.com/ars.)

showed that induction of Srx in the mouse liver in response to ethanol feeding is predominantly mediated *via* an Nrf2 pathway (2). We, therefore, examined whether the same pathway mediates the pyrazole-induced expression of Srx with the use of Nrf2 knockout ($Nrf2^{-/-}$) mice (Supplementary Fig. S2A). The pyrazole-induced expression of Srx at both protein (Fig. 2A, B) and mRNA (Supplementary Fig. S2B) levels was greatly attenuated in $Nrf2^{-/-}$ mice compared with that in wild-type animals, suggesting that Nrf2 plays a key role in this process. However, the fact that pyrazole-induced Srx expression was not totally abolished in the liver of $Nrf2^{-/-}$ mice suggested that other transcription factors such

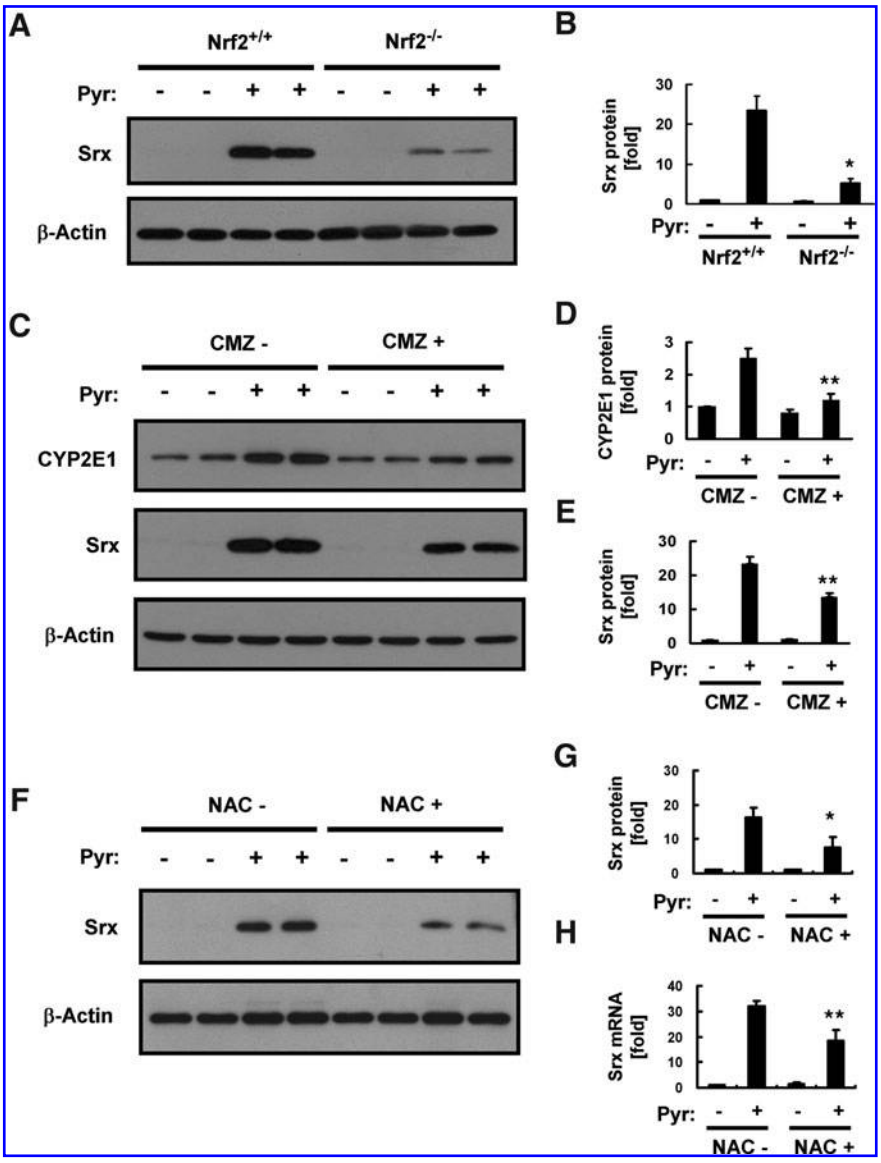

FIG. 2. Role of nuclear factor erythroid 2–related factor 2 (Nrf2) and CYP2E1 in pyrazole-induced Srx expression in the liver. (A) Homogenates (20 μg of protein) of the liver prepared from $Nrf2^{+/+}$ or $Nrf2^{-/-}$ mice 18 h after an intraperitoneal injection with saline (−) or pyrazole (150 mg/kg) were subjected to an immunoblot analysis with antibodies specific for either Srx or β-actin. Data are representative of three independent experiments. **(B)** Densitometric analysis of relative Srx abundance in immunoblots similar to those in **(A)**. Data are means ± SD. *$p < 0.01$ versus wild-type mice injected with pyrazole. **(C)** Wild-type mice were intraperitoneally injected first with chlormethiazole (CMZ, 50 mg/kg) or saline (−) and then 18 h later, with saline (−) or pyrazole (150 mg/kg). Liver homogenates (20 μg of protein) prepared 18 h after the second injection were subjected to an immunoblot analysis with antibodies to CYP2E1, to Srx, or to β-actin. Data are representative of three independent experiments. (**D**, **E**) Densitometric analysis of relative CYP2E1 **(D)** and Srx **(E)** abundance in immunoblots similar to those in **(C)**. Data are means ± SD. **$p < 0.05$ versus corresponding mice injected with pyrazole without the treatment of CMZ. **(F)** Wild-type mice were intraperitoneally injected with or without NAC (150 mg/kg) before the pyrazole injection (150 mg/kg). Liver homogenates (20 μg of protein) prepared 18 h after the pyrazole injection were subjected to an immunoblot analysis with antibodies specific for either Srx or β-actin. Data are representative of three independent experiments. **(G)** Densitometric analysis of Srx protein expression for the immunoblots similar to those in **(F)**. Data were normalized by the amount of β-actin and then expressed relative to the corresponding mean value for saline-injected mice. Data are mean ± SD. *$p < 0.03$ versus the corresponding mice injected with pyrazole without treatment of NAC. **(H)** Total RNA prepared from the liver tissue of mice treated as in **(F)** was subjected to RT and real-time PCR analysis for the determination of the amounts of Srx mRNA. Data were normalized by the amount of 18S rRNA and then expressed relative to the corresponding value for saline-injected mice. Data are mean ± SD. **$p < 0.05$ versus the corresponding mice injected with pyrazole without the treatment of NAC.

as AP-1 may contribute to the transcriptional activation of the Srx gene by pyrazole.

To determine whether the induction of Srx expression by pyrazole depends on CYP2E1 induction, we examined the effect of an earlier injection of mice with chlormethiazole, which inhibits CYP2E1 expression. Chlormethiazole attenuated the pyrazole-induced increase in the amount of CYP2E1 in the liver by ~90% (Fig. 2C, D), whereas it inhibited the pyrazole-induced up-regulation of Srx by ~40% (Fig. 2C, E). These results suggested that oxidative stress resulting from increased CYP2E1 expression is responsible, in part, for the induction of Srx expression by pyrazole. The role of oxidative stress is supported by the fact that a preinjection of N-acetyl-L-Cys significantly attenuated the expression levels of Srx protein and mRNA in the livers of pyrazole-treated mice. (Fig. 2F–H).

Pyrazole elicits selective accumulation of PrxIII–SO_2 in the liver of Srx-deficient mice

We next examined the effect of pyrazole on the hyperoxidation of 2-Cys Prxs in the liver of wild-type and Srx knockout ($Srx^{-/-}$) mice by immunoblot analysis with antibodies that recognize a specific sequence surrounding the C_P–SO_2H moiety (37). Given that the active site sequence is the same for 2-Cys Prxs (PrxI to IV) and that the sizes of PrxI and PrxII are identical, the sulfinic forms of PrxI and PrxII cannot be differentiated by immunoblot analysis. However, the sizes of PrxI/II, PrxIII, and PrxIV are sufficiently different for the discrimination by such an analysis. A pyrazole injection induced an approximately threefold increase in the amount of sulfinic PrxIII (PrxIII–SO_2) in the liver of wild-type mice (Fig. 3A, B). The intensity of the PrxIII–SO_2 band was slightly greater for the liver of $Srx^{-/-}$ mice than for that of $Srx^{+/+}$ mice before pyrazole treatment, and pyrazole induced an approximately fourfold increase in the intensity of this band in $Srx^{-/-}$ mice (Fig. 3A, B). The extent of PrxIII hyperoxidation was evaluated further by two-dimensional (2D) polyacrylamide gel electrophoresis (PAGE) followed by immunoblot analysis (Fig. 3C). Hyperoxidation of a Cys residue induces an acidic (leftward) shift in the position of proteins on 2D gels. The intensities of PrxIII spots suggest that 20% to 30% of PrxIII was hyperoxidized in the liver of pyrazole-treated $Srx^{-/-}$ mice. The amount of PrxI/II–SO_2 in the liver was not affected by either a pyrazole injection or Srx ablation alone, but it was slightly increased by pyrazole treatment in $Srx^{-/-}$ mice (Fig. 3A). Neither a pyrazole injection nor Srx ablation affected the expression levels of PrxI to IV (Fig. 3A). The amounts of glutathione peroxidase (Gpx), catalase, Zn- and Cu-dependent superoxide dismutase (SOD), and Mn-dependent SOD were also not affected by pyrazole treatment or Srx ablation (Fig. 3D).

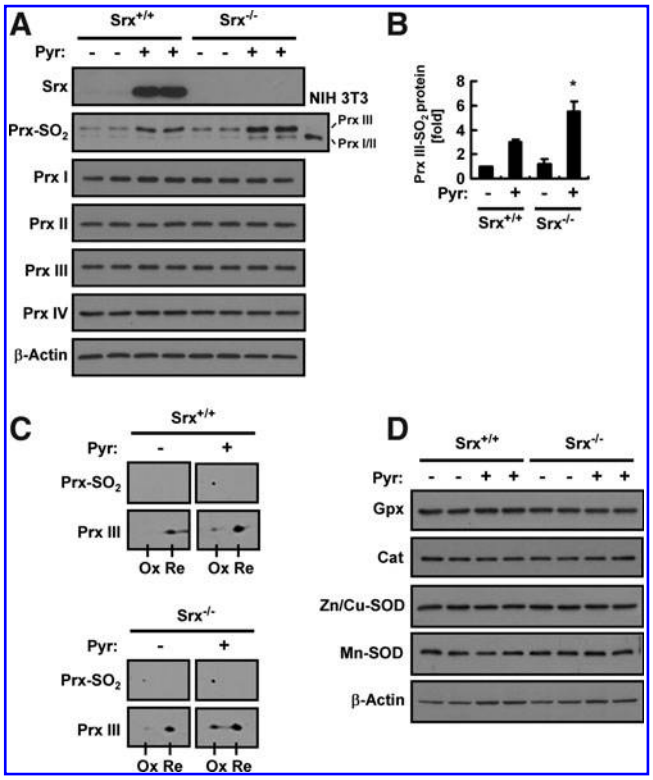

FIG. 3. Effects of pyrazole on the abundance and hyperoxidation of 2-cysteine (Cys) peroxiredoxins (Prxs) in the liver of $Srx^{+/+}$ or $Srx^{-/-}$ mice. (A) Liver homogenates (20 μg of protein) prepared 18 h after an intraperitoneal injection of $Srx^{+/+}$ or $Srx^{-/-}$ mice with saline (−) or pyrazole (150 mg/kg) were subjected to an immunoblot analysis with antibodies to Srx, to hyperoxidized 2-Cys Prxs (Prx–SO_2), to PrxI to IV, or to β-actin. A total lysate (5 μg of protein) of NIH 3T3 cells that had been treated with 100 μM H_2O_2 for 10 min was used as a positive control for hyperoxidized forms of PrxI/II and III. Data are representative of three independent experiments. **(B)** Densitometric analysis of PrxIII–SO_2 abundance in immunoblots similar to those in **(A)**. Data are means ± SD and are expressed relative to the normalized value for saline-injected $Srx^{+/+}$ mice. $^*p < 0.05$ versus pyrazole-injected $Srx^{+/+}$ mice. **(C)** Liver homogenates (250 μg of protein) prepared from mice treated as in **(A)** were subjected to two-dimensional polyacrylamide gel electrophoresis followed by an immunoblot analysis with antibodies specific for Prx–SO_2 and PrxIII. Ox and Re indicate spots corresponding to hyperoxidized and reduced forms, respectively, of PrxIII. **(D)** Liver homogenates (250 μg of protein) prepared from mice treated as in **(A)** were subjected to an immunoblot analysis with antibodies to glutathione peroxidase (Gpx), to catalase (Cat), to Zn- and Cu-dependent superoxide dismutase (Zn/Cu-SOD), to Mn-dependent superoxide dismutase (Mn-SOD), or to β-actin. Data are representative of three independent experiments.

Pyrazole increases CYP2E1 abundance in mitochondria to a greater extent than in ER and induces Srx translocation to both mitochondria and the ER

Both ethanol and pyrazole increase the abundance of CYP2E1 in the ER and mitochondria of rat liver (4, 29, 35). We find, however, that pyrazole induced the hyperoxidation of PrxIII but not that of PrxI and II in the liver. We, therefore, investigated whether the abundance of CYP2E1 in hepatic mitochondria might be increased to a greater extent than that in microsomes in pyrazole-injected mice. Liver homogenates prepared from pyrazole-treated mice were subjected to subcellular fractionation, and the abundance of CYP2E1 in the total homogenate, microsomal fraction, and mitochondrial fraction was examined by immunoblot analysis. The fidelity of the subcellular fractionation was confirmed by immunoblot analysis with antibodies to the 78-kDa glucose-regulated protein (GRP78, an ER marker) and those to cytochrome c

oxidase IV (COXIV, a mitochondrial marker). Pyrazole treatment induced 1.4- and 3.5-fold increases in the amount of CYP2E1 in the microsomal and mitochondrial fractions, respectively (Fig. 4A, B). A direct assay of CYP2E1 activity also indicated that pyrazole treatment increased CYP2E1 activity in the mitochondrial fraction to a greater extent than in the microsomal fraction (Fig. 4C). In addition, pyrazole treatment significantly increased lipid peroxidation in mitochondria but not in microsomes (Fig. 4D).

Srx is a cytosolic protein, but it translocates to the mitochondria in response to oxidative stress (3, 25). We previously showed that Srx also translocates to the cytosolic side of the ER membrane as well as to mitochondria in the liver of ethanol-fed mice (2). We, therefore, examined the effect of pyrazole treatment on the subcellular distribution of Srx in the liver. Srx was detected in the cytosol but not in the microsomal or mitochondrial fractions of the liver of control mice, whereas it was present in all three fractions of the liver of pyrazole-treated mice (Fig. 4E).

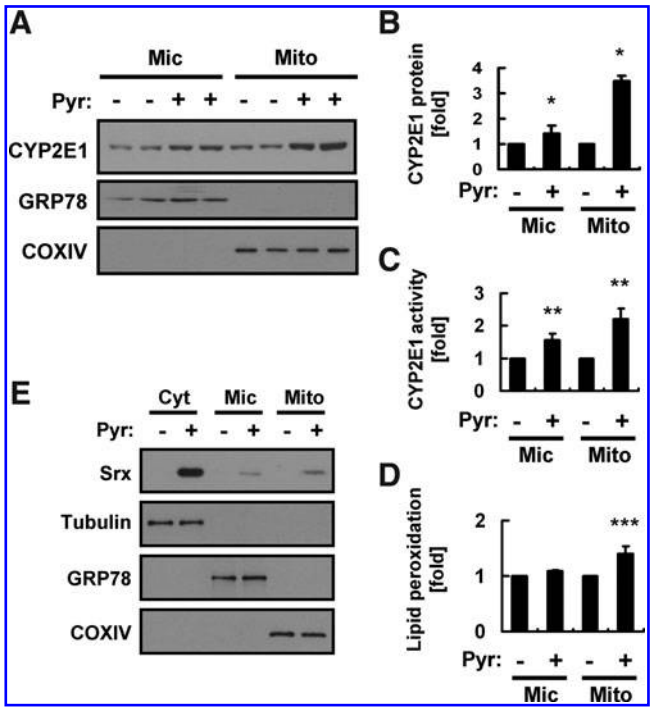

FIG. 4. Effects of pyrazole on the abundance or subcellular localization of CYP2E1 and Srx. (A) Liver homogenates prepared from mice 18 h after an intraperitoneal injection of either saline (−) or pyrazole (150 mg/kg) were fractionated into mitochondrial (Mito), microsomal (Mic), and cytosolic (Cyt) fractions. The Mic and Mito fractions (20 μg of protein) were subjected to an immunoblot analysis with antibodies to CYP2E1, to GRP78, or to cytochrome c oxidase IV (COXIV). Data are representative of three independent experiments. **(B)** Densitometric analysis of relative CYP2E1 abundance in immunoblots similar to those in **(A)**. Data are means ± SD. *$p < 0.05$ versus corresponding values for the control group. **(C)** CYP2E1 activity was measured in the Mito and Mic fractions prepared as in **(A)**. Data are means ± SD, $n = 3$. **$p < 0.05$ versus corresponding values for the control group. **(D)** The Mic and Mito fractions (20 μg of protein) were assayed for lipid peroxidation by measuring MDA with the use of a thiobarbituric acid–reactive substance (TBARS) assay kit (Cayman Chemical, Ann Arbor, MI). Data are expressed as relative values to the control group and are means ± SD, $n = 3$. ***$p < 0.05$ versus corresponding values for the control group. **(E)** Cyt, Mic, and Mito fractions (20 μg of protein) from the liver of mice treated as in **(A)** were subjected to an immunoblot analysis with antibodies to Srx as well as with those to the respective marker proteins β-tubulin, GRP78, and COXIV.

Pyrazole induces ER stress that results in the accumulation of Ca^{2+} and ROS in mitochondria

The larger effect of pyrazole on CYP2E1 abundance in mitochondria than in ER might account, in part, for the selective hyperoxidation of PrxIII that is apparent in the liver of pyrazole-treated mice. On the other hand, the relatively small difference in the amount of CYP2E1 in liver mitochondria versus that in microsomes might not be sufficient to account for such selectivity.

Pyrazole was previously shown to induce ER stress, as evidenced by an increase in the amount of GRP78, in mouse hepatocytes (13). We also found that the level of GRP78 was increased in the liver of pyrazole-treated mice (Supplementary Fig. S3A, B). ER stress results in phosphorylation of the α subunit of eukaryotic initiation factor 2 (eIF2α) by double-stranded RNA–activated protein kinase–like ER kinase (PERK) (22). Increased phosphorylation of eIF2α was also observed in the liver of pyrazole-treated mice (Supplementary Fig. S3A, B). In addition, pyrazole treatment increased the hepatic abundance of mRNAs for ER stress-related proteins, including those for GRP78, TRB3 (a mammalian ortholog of *Drosophila* Tribbles), and ER degradation–enhancing α-mannosidase–like protein (EDEM; Supplementary Fig. S3C).

The function of the ER is closely linked to that of mitochondria. These two organelles, thus, constitute a dynamic network that underlies intracellular Ca^{2+} signaling. ER stress often results in the increased loading of Ca^{2+} in mitochondria, and a protracted increase in the amount of Ca^{2+} in the matrix of mitochondria stimulates mitochondrial metabolism and disrupts the electron transport chain, leading to the increased production of ROS (9, 15, 22). We, therefore, investigated whether pyrazole might increase the level of Ca^{2+} in the mitochondria of HeLa (human cervical cancer) and Hepa1c1c7 (mouse hepatoma) cells with the use of the mitochondrion-specific Ca^{2+} indicator Rhod-2, which becomes enriched in mitochondria as a result of its positive charge. Treatment with the Ca^{2+} ionophore A23187 resulted in a marked increase in Rhod-2 fluorescence, indicative of mitochondrial Ca^{2+} accumulation, in both HeLa and Hepa1c1c7 cells (Fig. 5A, B). Treatment with pyrazole also induced mitochondrial Ca^{2+} accumulation, albeit at a slower rate than that observed with A23187 (Fig. 5A, B). We then measured the effect of pyrazole on ROS production in the mitochondria with the use of MitoSox Red, a mitochondrial-specific superoxide indicator. The respiratory chain complex I inhibitor rotenone was used as a positive control for superoxide generation. Pyrazole increased mitochondrial ROS in HeLa or Hepa1c1c7 cells, and the effect was blocked by ruthenium red, an inhibitor of mitochondrial calcium transport (Fig. 5C, D). These results suggested that pyrazole-induced ER stress might be responsible for the increase in mitochondrial ROS. Indeed, pyrazole induced ER stress, as indicated by the increased expression of GRP78 and

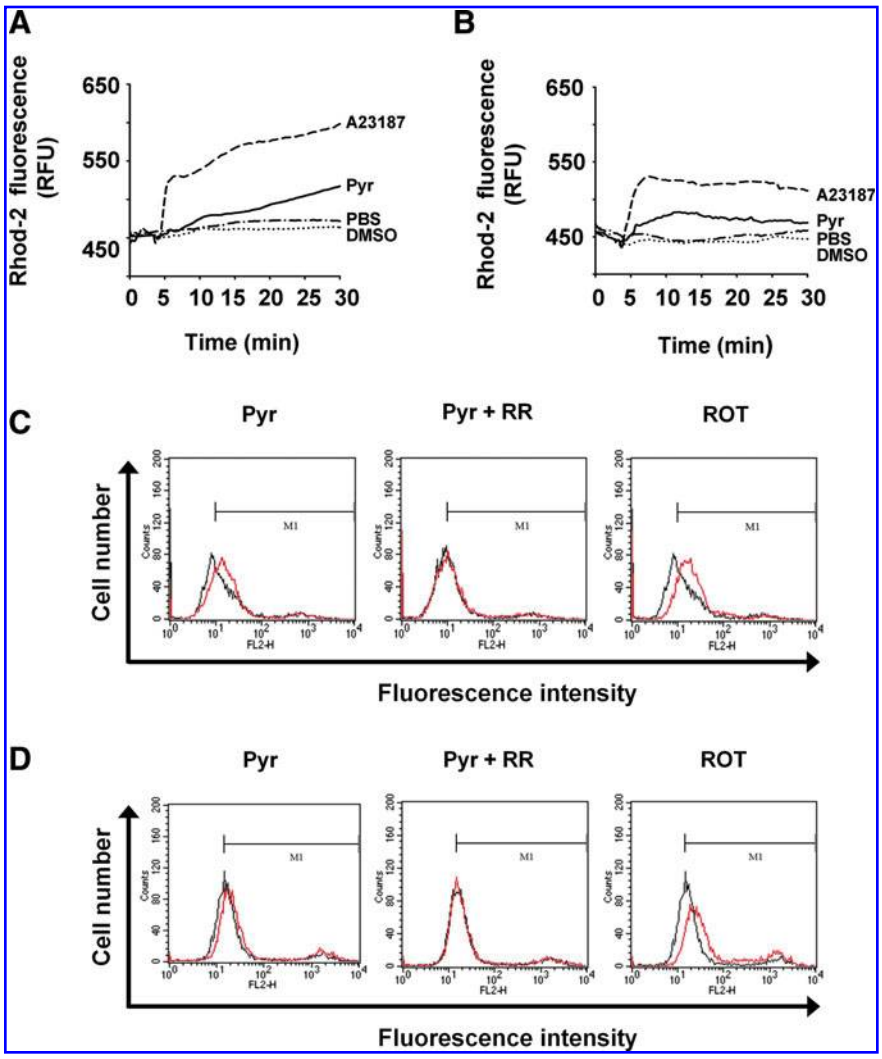

FIG. 5. Effects of pyrazole on the level of Ca^{2+} and reactive oxygen species (ROS) production in mitochondria of HeLa and Hepa1c1c7 cells. (A, B) HeLa **(A)** or Hepa1c1c7 **(B)** cells were exposed to A23187 (10 μM), DMSO, pyrazole (Pyr, 25 μM), or PBS. The amount of Mito Ca^{2+} was monitored as described under Supplementary Materials and Methods. Data are expressed as relative fluorescence units (RFU) and are from an experiment that was performed for a total of four times with similar results. **(C, D)** HeLa **(C)** or Hepa1c1c7 **(D)** cells were treated with pyrazole (100 μM), pyrazole (100 μM) plus ruthenium red (RR, 5 μM), or rotenone (ROT, 50 μM) in the presence of MitoSox Red dye (5 μM) for 30 min at 37°C and rinsed with PBS. The fluorescence intensity was measured by flow cytometry. The black line indicates the control group, and the red line indicates each treatment group.

of phosphorylation of eIF2α in HeLa or Hepa1c1c7 cells (Supplementary Fig. S4A–D). Pyrazole also increased protein carbonylation in the mitochondria of the two cell lines (Supplementary Fig. S4E, F).

Ablation of PrxIII or Srx exacerbates pyrazole-induced oxidative liver injury

Though mitochondria contain peroxide-eliminating enzymes such as Gpx and Prx V, ~90% of mitochondrial H_2O_2 was estimated to react with PrxIII (8). To elucidate the role of PrxIII in the protection of the liver from pyrazole-induced oxidative injury, we generated PrxIII knockout ($PrxIII^{-/-}$) mice (Supplementary Fig. S6) and examined the amount of carbonylated (oxidized) proteins in the liver of pyrazole-treated $PrxIII^{+/+}$ and $PrxIII^{-/-}$ mice. Carbonylated proteins were detected by derivatization of the carbonyl group with 2,4-dinitrophenylhydrazine (DNPH) followed by immunoblot analysis with antibodies to DNPH (Fig. 6A). Given that no protein bands were detected when DNPH was omitted from the derivatization mixture (Supplementary Fig. S7), the multiple bands apparent in each lane in Figure 6A likely represent carbonylated proteins. Pyrazole increased the level of protein carbonylation in the liver of both $PrxIII^{+/+}$ and $PrxIII^{-/-}$ mice, but a quantitative assay revealed that the extent of protein carbonylation in pyrazole-treated $PrxIII^{-/-}$ mice was 3.3 times that in pyrazole-treated $PrxIII^{+/+}$ mice (Fig. 6B). We next examined lipid peroxidation as revealed by detection of the markers 4-hydroxynonenal (4-HNE) and malondialdehyde (MDA). An immunohistochemical analysis showed that ablation of PrxIII markedly enhanced the pyrazole-induced formation of 4-HNE adducts in the centrilobular region of the liver of mice(Fig. 6C). Furthermore, the amount of MDA in the liver of pyrazole-treated $PrxIII^{-/-}$ mice was 2.4 times that in pyrazole-treated $PrxIII^{+/+}$ mice (Fig. 6D). Pyrazole also increased the frequency of apoptotic cell death in the liver of $PrxIII^{-/-}$ mice to a markedly greater extent than in that of $PrxIII^{+/+}$ mice (Fig. 6E, F).

Finally, we also investigated the role of Srx in protection of the liver from pyrazole-induced oxidative injury in the use of $Srx^{-/-}$ mice (Supplementary Fig. S5). Pyrazole induced protein carbonylation, 4-HNE adduct formation, and MDA production in the liver of $Srx^{-/-}$ mice to a greater extent than in that of $Srx^{+/+}$ mice (Fig. 7). The effects of Srx ablation appeared to be less pronounced than those of PrxIII ablation, however, as revealed by the 1.6- and 1.7-fold increases in

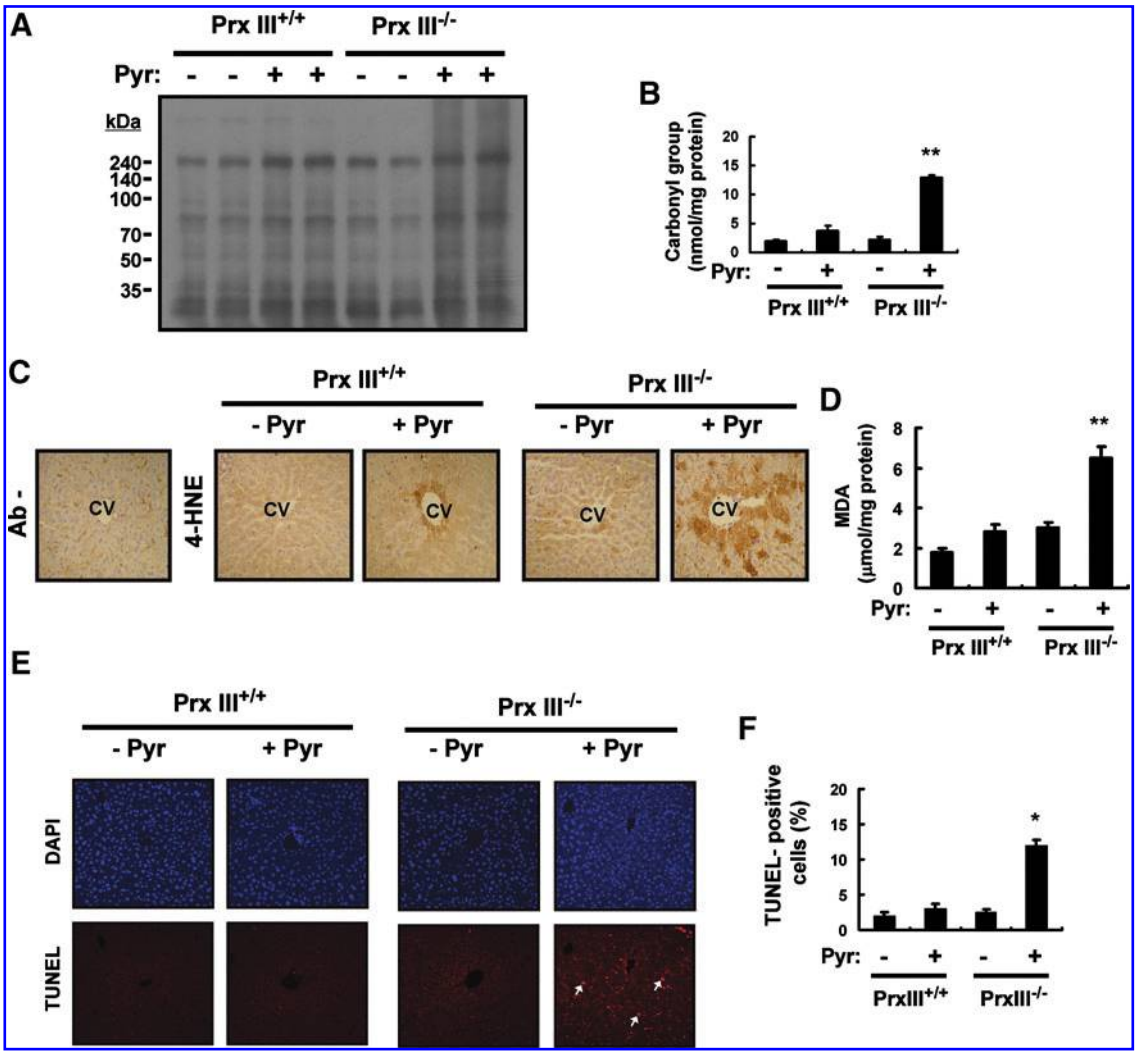

FIG. 6. Effects of PrxIII ablation on oxidative liver damage induced by pyrazole. (A) Liver homogenates (20 μg of protein) prepared from PrxIII$^{+/+}$ or PrxIII$^{-/-}$ mice 18 h after an intraperitoneal injection with saline (−) or pyrazole (150 mg/kg) were subjected to an immunoblot analysis of carbonylated proteins with the use of an Oxyblot Protein Oxidation Detection Kit (Chemicon, Temecula, CA). Molecular size markers are indicated in kilodaltons. Data are representative of three independent experiments. **(B)** Liver homogenates (20 μg of protein) from the mice treated as in **(A)** were subjected to an enzyme-linked immunosorbent assay for carbonylated proteins with the use of an OxyELISA Kit (Chemicon, Temecula, CA). Data are expressed as nanomoles of carbonyl group per milligram of protein and are means ± SD, $n = 3$. $^{**}p < 0.03$ versus pyrazole-treated PrxIII$^{+/+}$ mice. **(C)** Liver sections from the mice treated as in **(A)** were subjected to an immunohistochemical analysis with or without antibodies (Ab −) to 4-hydroxynonenal (4-HNE) with the use of an ABC staining kit (Vector Laboratories, Mississauga, Ontario, Canada). CV, central vein. Original magnification, 100×. **(D)** Liver homogenates (20 μg of protein) from mice treated as in **(A)** were assayed for MDA with the use of a TBARS assay kit (Cayman Chemical, Ann Arbor, MI). Data are expressed as micromoles per milligram of protein and are means ± SD, $n = 3$. $^{**}p < 0.03$ versus pyrazole-treated PrxIII$^{+/+}$ mice. **(E)** Liver sections from mice treated as in **(A)** were subjected to TUNEL analysis, which uses an *In Situ* Cell Death Detection Kit, TMR Red (Roche, Indianapolis, IN). The fluorescence signals were detected with a confocal microscope (LSM 510, Zeiss). *Arrows* indicate apoptotic cells. **(F)** The frequency of apoptotic cells in sections similar to those in **(E)** was quantified by counting the number of TUNEL-positive cells in 10 random microscopic fields and presenting them as the percentage of cells that were TUNEL positive. $^{*}p < 0.05$ versus pyrazole-treated PrxIII$^{+/+}$ mice. (To see this illustration in color the reader is referred to the web version of this article at www.liebertpub.com/ars.)

pyrazole-induced protein carbonylation (Fig. 7A, B) and MDA formation (Fig. 7D), respectively, compared with the corresponding values of 3.3- and 2.4-fold for PrxIII ablation.

Discussion

Pyrazole increases the abundance of CYP2E1. We have now shown that pyrazole also increases the levels of Srx protein and mRNA in the mouse liver. The availability of Nrf2$^{-/-}$ mice allowed us to show that pyrazole-induced Srx expression is largely dependent on Nrf2 function. Our results, thus, suggest that pyrazole stimulates the intracellular production of ROS by up-regulating CYP2E1 abundance, and that the generated ROS trigger the release of Nrf2 from Keap1 and its translocation to the nucleus, where it binds to the ARE in the promoter region of genes for various antioxidant

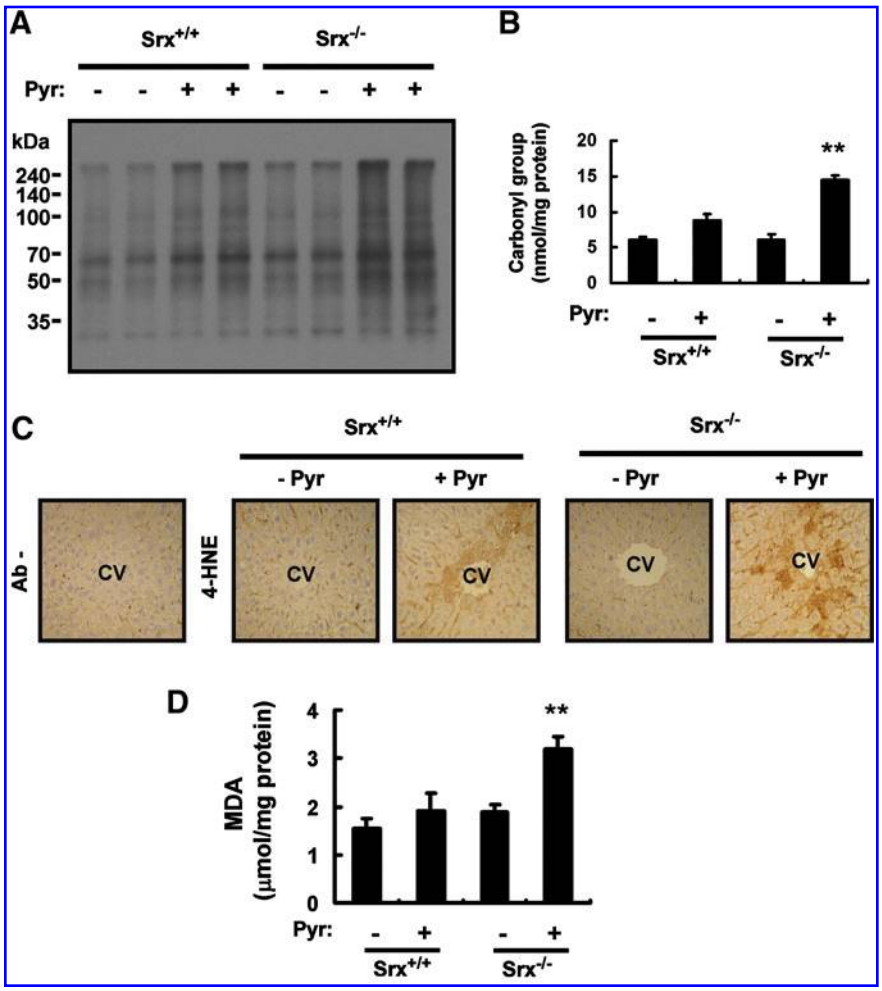

FIG. 7. Effects of Srx ablation on oxidative liver damage induced by pyrazole. (A) Liver homogenates (20 μg of protein) prepared from $Srx^{+/+}$ or $Srx^{-/-}$ mice 18 h after an intraperitoneal injection with saline (−) or pyrazole (150 mg/kg) were subjected to an immunoblot analysis of carbonylated proteins with the use of an Oxyblot Protein Oxidation Detection Kit (Chemicon, Temecula, CA). Data are representative of three independent experiments. **(B)** Liver homogenates (20 μg of protein) from mice treated as in **(A)** were subjected to an enzyme-linked immunosorbent assay for carbonylated proteins with the use of an OxyELISA Kit (Chemicon, Temecula, CA). Data are expressed as nanomoles of the carbonyl group per milligram of protein and are means ± SD, $n = 3$. $^{**}p < 0.01$ versus pyrazole-treated $Srx^{+/+}$ mice. **(C)** Liver sections from mice treated as in **(A)** were subjected to an immunohistochemical analysis with or without antibodies (Ab −) to 4-HNE with the use of an ABC staining kit (Vector Laboratories, Mississauga, Ontario, Canada). CV, central vein. Original magnification, 100×. **(D)** Liver homogenates (20 μg of protein) from mice treated as in **(A)** were assayed for MDA with the use of an OxyELISA Kit (Chemicon, Temecula, CA). Data are expressed as micromoles per milligram of protein and are means ± SD, $n = 3$. $^{**}p < 0.01$ versus pyrazole-treated $Srx^{+/+}$ mice. (To see this illustration in color the reader is referred to the web version of this article at www.liebertpub.com/ars.)

proteins, including Srx, thereby activating their transcription (Fig. 8). Although pyrazole-treated mice usually do not overt liver toxicity, pyrazole induces pronounced oxidative liver damage in $Nrf2^{-/-}$ mice (21). Such damage was attributed to the failure of these mice to induce compensatory increases in the abundance of Nrf2-regulated antioxidant enzymes such as γ-glutamylcysteine synthetase, heme oxygenase–1, and glutathione S-transferase (21). Our findings now suggest that Srx is also a key target of Nrf2 that is necessary to protect the liver from pyrazole-induced injury. Srx is a cytosolic protein that is able to translocate to sites where hyperoxidized (inactivated) 2-Cys Prxs are located, thereby engaging in reactivation of the inactivated enzymes under oxidative conditions (25). We have now shown that pyrazole treatment induced the translocation of Srx molecules to mitochondria and microsomes in the mouse liver (Fig. 8).

Among the four members of the 2-Cys Prx subgroup, only PrxIII was found to be hyperoxidized in the liver of pyrazole-treated wild-type mice, suggesting that the rate of hyperoxidation of PrxIII in mitochondria exceeded the capacity of Srx molecules which translocated to these organelles. In contrast, PrxI, but not PrxIII, was previously found to be hyperoxidized in the liver of ethanol-fed mice (2). Given that 2-Cys Prxs undergo hyperoxidation only when engaged in the catalytic cycle, the extent of PrxIII hyperoxidation is determined by the amount of ROS produced and the capacity of Srx to reverse the hyperoxidation. One of the major ROS sources responsible for PrxIII hyperoxidation in the liver of pyrazole-treated mice is CYP2E1, which, along with PrxIII, is present in the matrix of mitochondria (5, 7). A small proportion of PrxI molecules in microsomes was found to be hyperoxidized in the liver of pyrazole-treated $Srx^{-/-}$ mice, consistent with the notion that PrxI–SO_2 was not detected in the liver of pyrazole-treated $Srx^{+/+}$ mice, because the capacity of Srx located at the surface of the ER is sufficient to counteract the unavoidable hyperoxidation of PrxI. Despite the fact that both PrxI and PrxII exist in the cytosol and that PrxII is more prone to hyperoxidation than is PrxI, PrxII–SO_2 was not detected in the liver of pyrazole-treated wild-type or $Srx^{-/-}$ mice, suggesting that PrxII was not engaged in ROS elimination rather than that the capacity of Srx in the cytosol was sufficient to counteract its hyperoxidation.

CYP2E1 is an abundant protein in the liver that is predominantly located in microsomes. However, a substantial amount of CYP2E1 is also present in other cellular compartments, including mitochondria (4, 23, 29). The abundance of CYP2E1 in mitochondria and microsomes was increased 3.5- and 1.4-fold, respectively, in pyrazole-treated mice. It has been shown that mitochondrial CYP2E1 is more potent in generating ROS than the ER CYP2E1 (5, 31), probably because

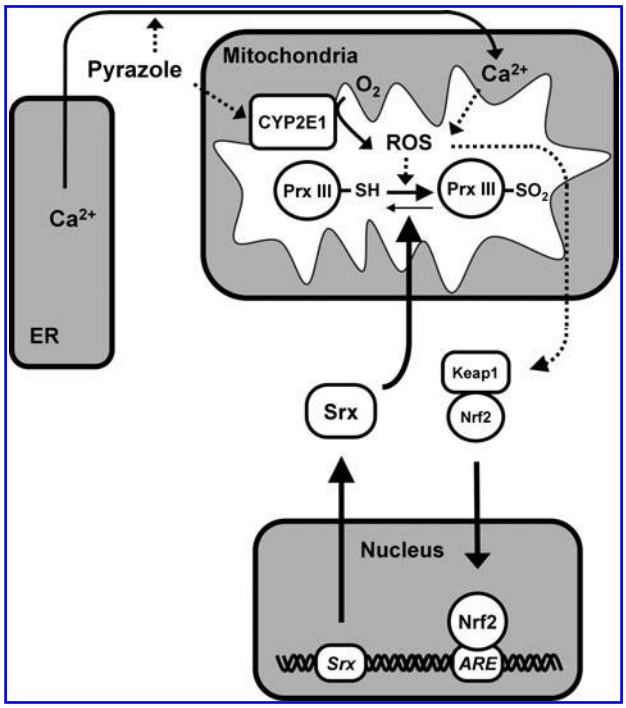

FIG. 8. Model for pyrazole-induced ROS production, PrxIII hyperoxidation, and Srx expression in mouse liver. See text for details.

CYP2E1 is more loosely coupled to its mitochondrial electron donor ferrodoxin compared with its ER electron donor cytochrome P450 reductase.

Our observation that chlormethiazole inhibited the pyrazole-induced up-regulation of Srx by only ~40% whereas it inhibited that of CYP2E1 by ~90% suggested the existence of a pyrazole-induced ROS source other than CYP2E1. Pyrazole is also thought to increase ROS levels in peroxisomes, given that the peroxisomal enzymes catalase and inducible nitric oxide synthase are inhibited and up-regulated, respectively, by pyrazole (21, 33). It is not likely, however, that the ROS produced in peroxisomes are able to travel to mitochondria, thereby promoting PrxIII hyperoxidation. Another CYP2E1-independent ROS source is mitochondria themselves, which are physically and functionally linked to the ER. These two organelles constitute a dynamic network that contributes to intracellular Ca^{2+} signaling. Pyrazole induces ER stress, which is known to result in Ca^{2+} leakage from the lumen of the ER (9, 15, 22). The Ca^{2+} released from the ER is taken up by mitochondria and becomes concentrated in the mitochondrial matrix. Indeed, with the use of the indicator Rhod-2, we have now shown that pyrazole induced Ca^{2+} accumulation in the mitochondria of HeLa and Hepa1c1c7 cells. Increased Ca^{2+} concentration stimulates mitochondrial ROS production through multiple mechanisms, including the activation of metabolism and the disruption of electron transport (9, 15, 22). Mitochondrial ROS can further increase Ca^{2+} release from the ER by sensitizing ER Ca^{2+}-release channels (9, 15, 22). The ER stress initiated by pyrazole, thus, triggers a positive feedback loop that results in the accumulation of Ca^{2+} and ROS in mitochondria (Fig. 8). The preferential hyperoxidationof PrxIII in pyrazole-treated mice is, therefore, attributable to the cumulative effect of the preferential induction of CYP2E1 and ER stress-derived ROS production in mitochondria.

The elimination of mitochondrial ROS by PrxIII is accompanied by PrxIII hyperoxidation, and the accumulation of inactive PrxIII results in the buildup of ROS in mitochondria. The overflow of excess ROS into the cytosol triggers Nrf2 activation (Fig. 8) and inflicts oxidative damage. Oxidative damage to the liver caused by pyrazole-induced ROS production can be assessed by the measurement of carbonylated proteins, 4-HNE adducts, and MDA (10, 14). The antioxidant role of PrxIII was, thus, evident from our findings that pyrazole-induced protein carbonylation as well as the formation of 4-HNE adducts and MDA in the liver were markedly increased in PrxIII$^{-/-}$ mice compared with wild-type mice. Increased mitochondrial production of ROS resulting from PrxIII ablation was also associated with apoptotic cell death in the liver of pyrazole-treated PrxIII$^{-/-}$ mice. Ablation of Srx also potentiated pyrazole-induced oxidative damage in the liver, albeit to a lesser extent than did PrxIII ablation, indicative of the key role of Srx as the guardian of 2-Cys Prxs.

Materials and Methods

Materials

Antibodies specific for PrxI to VI and for hyperoxidized 2-Cys Prxs (Prx–SO_2) were obtained from Young In Frontier (Seoul, Korea). Polyclonal antibodies to Srx were previously described (37), and a mouse monoclonal antibody to Srx was generated in house. Other antibodies were obtained from the following sources: β-actin (Sigma Aldrich, St. Louis, MO), GRP78 (Stressgen, Ann Arbor, MI), CYP2E1 (Abcam, Cambridge, UK), COXIV (Cell Signaling, Beverly, MA), 4-HNE (JaICA, Fukuroi, Japan), p-eIF2α, eIF2α (Cell Signaling, Danvers, MA), and β-tubulin (Santa Cruz Biotechnology, Santa Cruz, CA). Pyrazole, chlormethiazole, and rotenone were obtained from Sigma Aldrich (St. Louis, MO). A23187 was obtained from Invitrogen (Carlsbad, CA). Ruthenium red was obtained from Calbiochem (San Diego, CA).

Animals and treatments

All animals were housed with a 12-h-light, 12-h-dark cycle in a temperature-controlled environment. Male C57BL/6 mice and breeding pairs of Nrf2$^{-/-}$ mice were obtained from The Jackson Laboratory (Bar Harbor, ME) and RIKEN BioResource Center (Tsukuba, Japan), respectively. Overall, 8- to 10-week-old male mice were intraperitoneally injected with pyrazole (150 mg/kg) or saline, and, 18 h later, they were anesthetized by an intraperitoneal injection of pentobarbital (50 mg/kg), and the liver was perfused with phosphate-buffered saline, excised, and cut into fragments. All procedures were approved by the Animal Care and Use Committee of the Ewha Womans University.

RT-PCR analysis

Total RNA was isolated from liver tissue with the use of the Trizol reagent (Invitrogen, Carlsbad, CA). Portions (2 μg) of the RNA were subjected to RT with random hexamer primers and with the use of an ABI cDNA synthesis kit (PE Biosystems, Foster City, CA). For verification of the genotype of Nrf2 knockout mice, the resulting cDNA (1 μg) was subjected to

PCR analysis with the primers specific for Nrf2 and β-actin, as previously described (3). Real-time (quantitative) PCR analysis was performed with the use of 18S rRNA as an internal control. The primer sequences for Srx and PrxI to VI were previously described (11), as were those for TRB3, GRP78, and EDEM (16).

Subcellular fractionation and immunoblot analysis

Liver homogenates and subcellular fractions thereof were prepared as previously described (2). 2D gel electrophoresis and immunoblot analysis were also previously described (2). The abundance of target proteins was quantitated by a densitometric analysis of immunoblots with NIH ImageJ software.

CYP2E1 activity assay

The CYP2E1 activity in the mitochondrial or microsomal fraction was determined as described (29).

Statistical analysis

Unless indicated otherwise, quantitative data were presented as means ± standard deviation and were analyzed with the two-tailed Student's *t*-test. A *p*-value of <0.05 was considered statistically significant.

For additional details on Materials and Methods, please refer the Supplementary Data.

Acknowledgments

This study was supported by the National Honor Scientist program grant 2006-05106 (S.G.R) and the Bio R&D program grant M10642040001-07N4204-00110 (S.G.R.) from, as well as the BK21 program (S.H.B. and H.E.L.) of, the Korean government.

Author Disclosure Statement

No competing financial interests exist.

References

1. Anandatheerthavarada HK, Addya S, Dwivedi RS, Biswas G, Mullick J, and Avadhani NG. Localization of multiple forms of inducible cytochromes P450 in rat liver mitochondria: immunological characteristics and patterns of xenobiotic substrate metabolism. *Arch Biochem Biophys* 339: 136–150, 1997.
2. Bae SH, Sung SH, Cho EJ, Lee SK, Lee HE, Woo HA, Yu D, Kil IS, and Rhee SG. Concerted action of sulfiredoxin and peroxiredoxin I protects against alcohol-induced oxidative injury in mouse liver. *Hepatology* 53: 945–953, 2011.
3. Bae SH, Woo HA, Sung SH, Lee HE, Lee SK, Kil IS, and Rhee SG. Induction of sulfiredoxin via an Nrf2-dependent pathway and hyperoxidation of peroxiredoxin III in the lungs of mice exposed to hyperoxia. *Antioxid Redox Signal* 11: 937–948, 2009.
4. Bai J and Cederbaum AI. Overexpression of CYP2E1 in mitochondria sensitizes HepG2 cells to the toxicity caused by depletion of glutathione. *J Biol Chem* 281: 5128–5136, 2006.
5. Bansal S, Liu CP, Sepuri NB, Anandatheerthavarada HK, Selvaraj V, Hoek J, Milne GL, Guengerich FP, and Avadhani NG. Mitochondria-targeted cytochrome P450 2E1 induces oxidative damage and augments alcohol-mediated oxidative stress. *J Biol Chem* 285: 24609–24619, 2010.
6. Biteau B, Labarre J, and Toledano MB. ATP-dependent reduction of cysteine-sulphinic acid by S. cerevisiae sulphiredoxin. *Nature* 425: 980–984, 2003.
7. Cox AG, Peskin AV, Paton LN, Winterbourn CC, and Hampton MB. Redox potential and peroxide reactivity of human peroxiredoxin 3. *Biochemistry* 48: 6495–6501, 2009.
8. Cox AG, Winterbourn CC, and Hampton MB. Mitochondrial peroxiredoxin involvement in antioxidant defence and redox signaling. *Biochem J* 425: 313–325, 2009.
9. Deniaud A, Sharaf el dein O, Maillier E, Poncet D, Kroemer G, Lemaire C, and Brenner C. Endoplasmic reticulum stress induces calcium-dependent permeability transition, mitochondrial outer membrane permeabilization and apoptosis. *Oncogene* 27: 285–299, 2008.
10. Dey A and Cederbaum AI. Induction of cytochrome P450 2E1 [corrected] promotes liver injury in ob/ob mice. *Hepatology* 45: 1355–1365, 2007.
11. Diet A, Abbas K, Bouton C, Guillon B, Tomasello F, Fourquet S, Toledano MB, and Drapier JC. Regulation of peroxiredoxins by nitric oxide in immunostimulated macrophages. *J Biol Chem* 282: 36199–36205, 2007.
12. Fisher AB. Peroxiredoxin 6: a bifunctional enzyme with glutathione peroxidase and phospholipase A2 activities. *Antioxid Redox Signal* 15: 831–844, 2011.
13. Gilmore WJ and Kirby GM. Endoplasmic reticulum stress due to altered cellular redox status positively regulates murine hepatic CYP2A5 expression. *J Pharmacol Exp Ther* 308: 600–608, 2004.
14. Gong P and Cederbaum AI. Nrf2 is increased by CYP2E1 in rodent liver and HepG2 cells and protects against oxidative stress caused by CYP2E1. *Hepatology* 43: 144–153, 2006.
15. Gorlach A, Klappa P, and Kietzmann T. The endoplasmic reticulum: folding, calcium homeostasis, signaling, and redox control. *Antioxid Redox Signal* 8: 1391–1418, 2006.
16. Kammoun HL, Chabanon H, Hainault I, Luquet S, Magnan C, Koike T, Ferre P, and Foufelle F. GRP78 expression inhibits insulin and ER stress-induced SREBP-1c activation and reduces hepatic steatosis in mice. *J Clin Invest* 119: 1201–1215, 2009.
17. Kessova I and Cederbaum AI. CYP2E1: biochemistry, toxicology, regulation and function in ethanol-induced liver injury. *Curr Mol Med* 3: 509–518, 2003.
18. Knoops B, Goemaere J, Van der Eecken V, and Declercq JP. Peroxiredoxin 5: structure, mechanism, and function of the mammalian atypical 2-Cys peroxiredoxin. *Antioxid Redox Signal* 15: 817–829, 2011.
19. Lieber CS. Cytochrome P-4502E1: its physiological and pathological role. *Physiol Rev* 77: 517–544, 1997.
20. Lu Y and Cederbaum AI. CYP2E1 and oxidative liver injury by alcohol. *Free Radic Biol Med* 44: 723–738, 2008.
21. Lu Y, Gong P, and Cederbaum AI. Pyrazole induced oxidative liver injury independent of CYP2E1/2A5 induction due to Nrf2 deficiency. *Toxicology* 252: 9–16, 2008.
22. Malhotra JD and Kaufman RJ. Endoplasmic reticulum stress and oxidative stress: a vicious cycle or a double-edged sword? *Antioxid Redox Signal* 9: 2277–2293, 2007.
23. Neve EP and Ingelman-Sundberg M. A soluble NH(2)-terminally truncated catalytically active form of rat cytochrome P450 2E1 targeted to liver mitochondria. *FEBS Lett* 460: 309–314, 1999.
24. Neve EP and Ingelman-Sundberg M. Identification and characterization of a mitochondrial targeting signal in rat

cytochrome P450 2E1 (CYP2E1). *J Biol Chem* 276: 11317–11322, 2001.
25. Noh YH, Baek JY, Jeong W, Rhee SG, and Chang TS. Sulfiredoxin Translocation into Mitochondria Plays a Crucial Role in Reducing Hyperoxidized Peroxiredoxin III. *J Biol Chem* 284: 8470–8477, 2009.
26. Rabilloud T, Heller M, Gasnier F, Luche S, Rey C, Aebersold R, Benahmed M, Louisot P, and Lunardi J. Proteomics analysis of cellular response to oxidative stress. Evidence for *in vivo* overoxidation of peroxiredoxins at their active site. *J Biol Chem* 277: 19396–19401, 2002.
27. Rashba-Step J, Turro NJ, and Cederbaum AI. Increased NADPH- and NADH-dependent production of superoxide and hydroxyl radical by microsomes after chronic ethanol treatment. *Arch Biochem Biophys* 300: 401–408, 1993.
28. Rhee SG and Woo HA. Multiple functions of peroxiredoxins: peroxidases, sensors and regulators of the intracellular messenger H2O2, and protein chaperones. *Antioxid Redox Signal* 15: 781–794, 2011.
29. Robin MA, Anandatheerthavarada HK, Fang JK, Cudic M, Otvos L, and Avadhani NG. Mitochondrial targeted cytochrome P450 2E1 (P450 MT5) contains an intact N terminus and requires mitochondrial specific electron transfer proteins for activity. *J Biol Chem* 276: 24680–24689, 2001.
30. Sakurai K and Cederbaum AI. Oxidative stress and cytotoxicity induced by ferric-nitrilotriacetate in HepG2 cells that express cytochrome P450 2E1. *Mol Pharmacol* 54: 1024–1035, 1998.
31. Sangar MC, Bansal S, and Avadhani NG. Bimodal targeting of microsomal cytochrome P450s to mitochondria: implications in drug metabolism and toxicity. *Expert Opin Drug Metab Toxicol* 6: 1231–1251, 2010.
32. Song BJ. Ethanol-inducible cytochrome P450 (CYP2E1): biochemistry, molecular biology and clinical relevance: 1996 update. *Alcohol Clin Exp Res* 20: 138A–146A, 1996.
33. Stolz DB, Zamora R, Vodovotz Y, Loughran PA, Billiar TR, Kim YM, Simmons RL, and Watkins SC. Peroxisomal localization of inducible nitric oxide synthase in hepatocytes. *Hepatology* 36: 81–93, 2002.
34. Tavender TJ, Sheppard AM, and Bulleid NJ. Peroxiredoxin IV is an endoplasmic reticulum-localized enzyme forming oligomeric complexes in human cells. *Biochem J* 411: 191–199, 2008.
35. Winters DK and Cederbaum AI. Time course characterization of the induction of cytochrome P-450 2E1 by pyrazole and 4-methylpyrazole. *Biochim Biophys Acta* 1117: 15–24, 1992.
36. Woo HA, Chae HZ, Hwang SC, Yang KS, Kang SW, Kim K, and Rhee SG. Reversing the inactivation of peroxiredoxins caused by cysteine sulfinic acid formation. *Science* 300: 653–656, 2003.
37. Woo HA, Jeong W, Chang TS, Park KJ, Park SJ, Yang JS, and Rhee SG. Reduction of cysteine sulfinic acid by sulfiredoxin is specific to 2-cys peroxiredoxins. *J Biol Chem* 280: 3125–3128, 2005.
38. Wu D and Cederbaum AI. Cytochrome P4502E1 sensitizes to tumor necrosis factor alpha-induced liver injury through activation of mitogen-activated protein kinases in mice. *Hepatology* 47: 1005–1017, 2008.
39. Wu D and Cederbaum AI. Ethanol and arachidonic acid produce toxicity in hepatocytes from pyrazole-treated rats with high levels of CYP2E1. *Mol Cell Biochem* 204: 157–167, 2000.
40. Yang KS, Kang SW, Woo HA, Hwang SC, Chae HZ, Kim K, and Rhee SG. Inactivation of human peroxiredoxin I during catalysis as the result of the oxidation of the catalytic site cysteine to cysteine-sulfinic acid. *J Biol Chem* 277: 38029–38036, 2002.

Address correspondence to:
Dr. Soo Han Bae
Division of Life and Pharmaceutical Sciences
Ewha Womans University
11-1 Daehyun-dong
Seodaemun-gu
Seoul 120-750
Korea

E-mail: soohanbae@ewha.ac.kr

Dr. Sue Goo Rhee
Division of Life and Pharmaceutical Sciences
Ewha Womans University
11-1 Daehyun-dong
Seodaemun-gu
Seoul 120-750
Korea

E-mail: rheesg@ewha.ac.kr

Date of first submission to ARS Central, October 28, 2011; date of final revised submission, April 9, 2012; date of acceptance, April 10, 2012.

Abbreviations Used

ARE = antioxidant-responsive element
COXIV = cytochrome c oxidase IV
Cys = cysteine
DNPH = 2,4-dinitrophenylhydrazine
EDEM = ER degradation–enhancing α-mannosidase–like protein
eIF2 = eukaryotic initiation factor 2
ER = endoplasmic reticulum
Gpx = glutathione peroxidase
GRP = glucose-regulated protein
4-HNE = 4-hydroxynonenal
MDA = malondialdehyde
Nrf2 = nuclear factor erythroid 2–related factor 2
PCR = polymerase chain reaction
Prx = peroxiredoxin
ROS = reactive oxygen species
RT = reverse transcription
Srx = sulfiredoxin